Polymer 51 (2010) 2708–2720

Contents lists available at ScienceDirect

Polymer

journal homepage: www.elsevier.com/locate/polymer

Analysis of agglomerate dispersion mechanisms of multiwalled carbon nanotubes during melt mixing in polycarbonate

Gaurav R. Kasaliwal, Sven Pegel, Andreas Göldel, Petra Pötschke*, Gert Heinrich

Leibniz Institute of Polymer Research Dresden, Hohe Str. 6, 01069 Dresden, Germany

ARTICLE INFO

Article history:
Received 18 December 2009
Received in revised form
22 February 2010
Accepted 26 February 2010
Available online 12 March 2010

Keywords:
Multiwalled carbon nanotubes
Polymer composites
Dispersion

ABSTRACT

Dispersion of primary nanotube agglomerates in polymer melts is one of the difficult tasks when applying melt mixing for nanocomposite preparation. Hence, there is a need for a better understanding of the ongoing processes. Filler agglomerates generally undergo dispersion by rupture and erosion mechanisms, which usually occur simultaneously. To analyse these mechanisms and their corresponding dispersion kinetics 1 wt% multiwalled carbon nanotubes (MWNT) were incorporated into polycarbonate using a microcompounder. Different mixing speeds at constant melt temperature were applied thereby changing the applied stress. The states of MWNT agglomerate dispersion at different mixing times were assessed by quantifying the agglomerate area ratio and particle size distribution using image analysis of optical transmission micrographs. A model is proposed to estimate the fractions of rupture and erosion mechanisms during agglomerate dispersion. At low mixing speeds, the dispersion was found to be governed by both mechanisms, whereas rupture dominance increases with increasing mixing speed. Further, the relationship between electrical resistivity and dispersion was studied indicating a critical behaviour. A dependency on the amount of dispersed nanotubes was found only in a certain range of state of dispersion.

1. Introduction

In recent years, manufacturing of polymer-multiwalled carbon nanotubes (MWNT) composites has acquired a lot of attention due to the extraordinary properties of MWNT. In this context, the state of MWNT dispersion in a polymer matrix plays a decisive role for the application of polymer–MWNT composites. A high cohesive strength of the "as produced" primary MWNT agglomerates restricts their dispersion into individualized tubes within the polymer matrix during melt compounding. This leads in many cases to the presence of un-dispersed MWNT agglomerates in composites as shown e.g. in [1–8]. The dispersive mixing operation during melt compounding of polymer-filler systems consists of several stages, namely filler incorporation, wetting and infiltration (by polymer melt), followed by dispersion, distribution, and flocculation (of filler in the polymer melt). During the stage of filler dispersion, the large initial filler agglomerates are reduced in size up to the smallest dispersible unit. In a first approximation, the change in size of large agglomerates into smaller parts can be attributed to two mechanisms, namely rupture (a bulk phenomenon) and erosion (a surface phenomenon). In rupture mechanism, the large agglomerates are broken down into smaller ones in short times; whereas in erosion mechanism, large agglomerates are eroded into smaller ones by removing single or bundles of nanotubes from the agglomerate surface needing comparatively longer time. As the dispersion step is the most difficult one, it is considered to determine the rate at which filler disperses in the polymer melt [9]. Therefore, it is necessary to investigate the melt compounding conditions that can govern such underlying dispersion mechanisms of MWNT agglomerates in the polymer melt.

For fillers like carbon black (CB), silica, calcium carbonate ($CaCO_3$), etc. such kinds of dispersion mechanisms have been extensively investigated and reported. Kao and Mason [10] and later Powell and Mason [11] studied the process of dispersion of non-cohesive clusters (made of lucite and polystyrene) in silicon oil under pure shear flow. They observed dispersion by erosion mechanism and proposed a model, stating that the rate at which particles leave the surface of the cluster is proportional to the surface area of the cluster. An "onion peeling model" of CB dispersion in rubber which seems to be similar to erosion mechanism was proposed by Shiga and Furuta [12]. They stated that aggregates could be dispersed by either individually or collectively scraping from the surface of agglomerates. For dispersion of

* Corresponding author. Tel.: +49 351 4658 395; fax: +49 351 4858 565.
E-mail address: poe@ipfdd.de (P. Pötschke).

0032-3861/$ – see front matter © 2010 Elsevier Ltd. All rights reserved.
doi:10.1016/j.polymer.2010.02.048

agglomerates by "rupture" mechanism, Bolen and Colwell [13] proposed that it occurs when shearing stresses exceed a certain threshold value dependent on the properties of filler. Later, extensive work has been reported on agglomerate dispersion mechanisms by the group of Manas-Zloczower and Feke [14–23]. One of the findings reported by them [16–18] reveals that in the course of CB dispersion, rupture mechanism generates a lower number of coarse fragments than erosion. Moreover, they stated that the critical shear stress required for dispersion by erosion process is much lower than the one required for the rupture process and based on an earlier reported work [24] they emphasised that the ratio of applied shear stress and cohesive strength of agglomerates could be decisive in agglomerate dispersion. This ratio was named as fragmentation number (Fa) by Hansen et al. [25]. The same group stated that the mechanism of agglomerate dispersion is dependent on a certain critical value of applied shear stress [26]. If Fa is smaller than $Fa_{critical}$, particles undergo dispersion by erosion and if Fa is larger than $Fa_{critical}$, particles undergo dispersion by rupture. Further, Potente et al. [27] proposed a mathematical model for the dispersion mechanisms which was used to simulate the dispersion process. A comparison was made with experimental data for the dispersion of $CaCO_3$ in polypropylene. Although the simulated and experimental results of degree of dispersion along screw length showed some deviations, the tendencies were similar. In a parallel work, Lozano et al. [28] proposed a model for dispersion mechanisms to simulate the particle size distribution of $CaCO_3$ in polypropylene. The predicted values could be fitted with the experimental values by assuming share of both dispersion mechanisms by trial and error method. Although both models consider dispersion by erosion and rupture mechanism, they do not directly quantify the share of both mechanisms during agglomerate dispersion.

Recently, we reported the influence of melt processing conditions on electrical resistivity and morphology of polycarbonate (PC)–MWNT composites [8]. It was stated that depending on compounding conditions, MWNT agglomerates could be dispersed by either rupture or erosion dominated mechanisms. In the prevailing work, to distinctly differentiate the occurrence of these dispersion mechanisms the dispersion kinetics of MWNT agglomerates was investigated by melt compounding PC with 1 wt% MWNT. Three different mixing speeds were employed, thereby applying three different shear rates, using a small scale DACA microcompounder. The effects on agglomerate size distribution and evolution of morphology due to different mixing conditions are reported. In any melt compounding process, filler agglomerate particles are subjected to dispersion by both rupture and erosion mechanisms as both mechanisms run parallel. A model is proposed to quantify the splitting of dispersion mechanisms during a melt mixing process into rupture and erosion. Furthermore, we report about electrical resistivities of composites produced under different mixing conditions.

2. Experimental

2.1. Materials

The MWNT used in this work (Baytubes® C150HP, Bayer MaterialScience AG, Germany) are produced by a catalytic chemical vapour deposition process and were supplied as agglomerates. The carbon purity of this highly purified material is >99%, the outer mean nanotube diameter is reported to be in the range of 13–16 nm, the length of the tubes is in the range of 1–10 μm, and their bulk density is 140–230 kg/m^3 [29].

As PC, a low viscosity grade Makrolon® 2205 (Bayer MaterialScience AG, Germany) (MVR 36 cm^3/10 min @ 300 °C) with a density of 1.2 g/cm^3 was selected. Before melt mixing, both PC and MWNT were dried overnight at 100 °C in vacuum.

2.2. Composite preparation

2.2.1. Melt compounding

A DACA microcompounder (DACA Instruments, Goleta, CA) representing a small scale conical, co-rotating twin-screw compounder with a volume of 4.5 cm^3 was used to melt mix the PC–MWNT nanocomposites. Mixing parameters such as barrel temperature (mixing temperature), rotation speed (mixing speed), and mixing time can be easily controlled, and the torque values can be monitored. The material is added stepwise in the running microcompounder and a charge of 4.2 g material was processed during each experiment.

As mentioned in a previous study, Baytubes C150HP show electrical percolation in PC at around 1 wt% addition when incorporated using the DACA microcompounder [8]. Thus, the concentration of 1 wt% was used to produce composites in three series by employing mixing speeds of 50, 100, and 300 rpm. The mixing temperature was set at 280 °C. To investigate the dispersion kinetics of MWNT agglomerates, in each series the mixing was done for 14 different mixing times namely 0.5, 2, 3, 5, 7, 9, 12, 15, 18, 20, 25, 30, 35, and 40 min. After mixing for the desired time, the entire material was taken out as a strand (diameter ~2 mm) using the set mixing speeds through the heated cylindrical die into air without additional cooling or drawing. The applied specific mixing energy was calculated using the torque values recorded during mixing following the procedure given in [8].

2.2.2. Compression moulding

In order to perform electrical measurements on defined geometries the extruded strands were compression moulded into circular plates using a Weber hot press (Model PW 40 EH, Paul Otto Weber GmbH, Remshalden, Germany). A circular frame of 60 mm diameter and 0.5 mm thickness was used as a forming tool. Compression moulding was carried out following the detailed procedure explained in [8]. The moulding was carried out at 265 °C for a pressing time of 1 min and a pressing speed of 6 mm/s.

2.3. Characterization of MWNT base material

2.3.1. Particle size analysis

The agglomerate size distribution of the as delivered MWNT powder was determined by laser diffraction using a Helos/BF particle size analyser coupled with a RODOS dry dispersion unit and an ASPIROS micro dose module (Sympatec GmbH, Clausthal-Zellerfeld, Germany). A pressure of 0.5 bar was used for the measurements. The measurement range of the equipment is 4.5–875 μm. The volume weighted agglomerate size distributions were calculated in accordance to the Fraunhofer method.

2.3.2. SEM investigation

Scanning electron microscopy (SEM) of as delivered MWNT agglomerates was carried out using a Carl Zeiss – Ultra plus scanning electron microscope (Carl Zeiss SMT, Ford Lauderdale, USA). The un-sputtered MWNT agglomerates were placed directly on an aluminium sample holder coated with conductive silver paste.

2.4. Composite characterization

2.4.1. Optical microscopy

The state of CNT dispersion has been characterized by transmission optical microscopy.

For each sample a series of thin sections with 20 microns thickness was prepared from extruded strands (perpendicular to the extrusion direction) using a RM 2055 microtome (Leica, Germany) at room temperature. A glass knife with a cut angle of 35° was used. Transmission microscopy was performed on these thin sections and the micrographs were imaged with a BH2 microscope equipped with a camera DP71 (both Olympus), using 10× objective and 20× ocular magnifications considering the entire cross-sectional area.

The optical micrographs have been analysed by means of the digital image processing software ImageJ. The cumulative area of the projected CNT agglomerate system has been used as one quantity to characterize state of dispersion. Principally, in case of thin sections this quantity reflects the agglomerate volume fraction only indirectly, since the number of agglomerates involved into the projection increases depending on the section thickness and the mean agglomerate size [30]. However, in the present case the error is small compared to the observed effects. From the cumulative area, the agglomerate area ratio *A* has been determined by relating to the micrograph area and this ratio is discussed in percentage. Further, all un-dispersed agglomerates are classified as per size classes based on their area equivalent diameters (each size class has the width of 10 μm). For agglomerates from each size class, their number (per mm^2) and their area ratio (cumulative area in that size class related to the micrograph area) were evaluated. Agglomerates with diameters smaller than 1 μm were not used for interpretation.

To have a sufficient statistics of measured values, at least eight images from four different positions along the length of the strand were used for analysis, leading to an investigated area of at least 4.8 mm^2.

2.4.2. Transmission electron microscopy

TEM was performed using a Carl Zeiss Libra transmission electron microscope on 80–100 nm thin sections cut at room temperature from extruded strands (perpendicular to extrusion direction). For imaging, an acceleration voltage of 120 KV and a zero loss filter were employed.

2.4.3. Electrical volume resistivity measurement

Electrical volume resistivity measurements were performed either on compression moulded circular plates (diameter: 60 mm, thickness 0.5 mm) or on strips cut from these plates, depending upon their resistivity values. For high resistivity samples (resistivity $> 10^7$ Ω cm), a Keithley Electrometer 6517A combined with an 8009 Resistivity Test Fixture equipped with ring electrodes was used. For samples having lower volume resistivity, the measurements were performed on strips (length ~20 mm, width ~7 mm) cut from the compression moulded plates, using a four-point test fixture combined with a Keithley Multimeter DMM 2000. The four-point test fixture has gold contact wires with a distance of 16 mm between the source electrodes and 10 mm between the measuring electrodes. The volume resistivity was measured at 24 °C and 40% relative humidity. Before measurements, the surfaces of the samples were cleaned with ethanol. For each specimen, two measurements were made for the high resistivity samples, and four measurements were made for the low resistivity samples.

3. Results and discussion

3.1. MWNT characterization

MWNT (Baytubes C150HP) agglomerates were characterized in order to know the initial state of particle size distribution and to have a visual impression of agglomerates before melt compounding is carried out. In Fig. 1, the particle size distribution of Baytubes C150HP is shown. The maximum agglomerate diameter was observed to be around 600 μm and the mean agglomerate size to be approx. 282 μm. In Fig. 2, SEM images of Baytubes C150HP as delivered material are shown. At low magnification, agglomerates of different sizes appear to be quite compact with a smooth surface. However, when looking deeper inside a fractured agglomerate surprisingly a substructure was observed revealing small agglomerates in the size range between 1 and 10 microns.

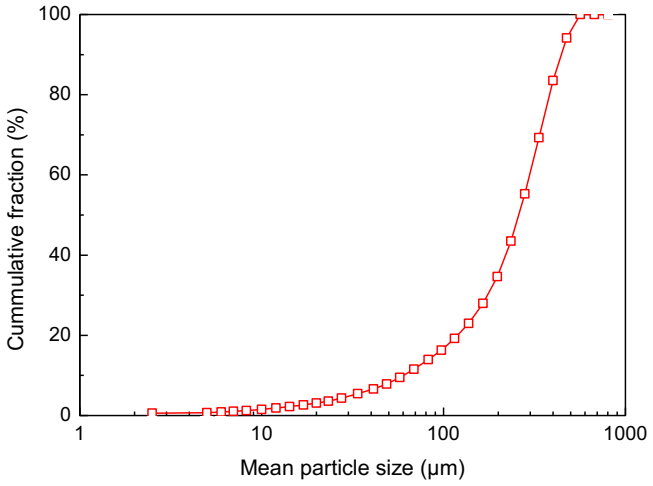

Fig. 1. Cumulative volume weighted distribution agglomerate sizes of (as delivered) Baytubes C150HP.

It should be noted that most of the works discussed in the literature concerning mechanisms of filler dispersion are based on dimensional changes observed on a single agglomerate or pellet and in some instances on narrow size distributed agglomerates. On the contrary, the work presented here is based on filler having a broad particle size distribution.

3.2. Kinetics of MWNT agglomerate dispersion

3.2.1. Optical microscopy investigations

To investigate the kinetics of MWNT agglomerate dispersion, 1 wt% MWNT was melt compounded with polycarbonate at mixing speeds of 50, 100, and 300 rpm; at a temperature of 280 °C, and different mixing times. The state of MWNT agglomerates dispersion at these three mixing speeds with increasing mixing time was evaluated by performing optical microscopy investigations on extruded strands as shown in Fig. 3.

From the micrographs, a decrease in size and number of agglomerates with mixing time is visible which is more pronounced when increasing mixing speed. To evaluate the size distribution of un-dispersed agglomerates such optical micrographs were quantitatively evaluated by applying an image analysis procedure.

In Fig. 4, the agglomerate size distributions are presented by plotting the number of agglomerates (per mm^2) versus the mean agglomerate diameter of each size class. The order of the plots corresponds to the images in Fig. 3.

It is generally observed that in composites prepared at low mixing speeds, a higher number of relatively larger agglomerates are present. The number of large agglomerates is reduced with increasing mixing speed and mixing time, thereby narrowing the size distribution of the un-dispersed agglomerates. The drastic decrease in the number of agglomerates from larger diameter classes indicates a relatively fast break-up of bigger agglomerates into smaller agglomerates. This results in the largest number of

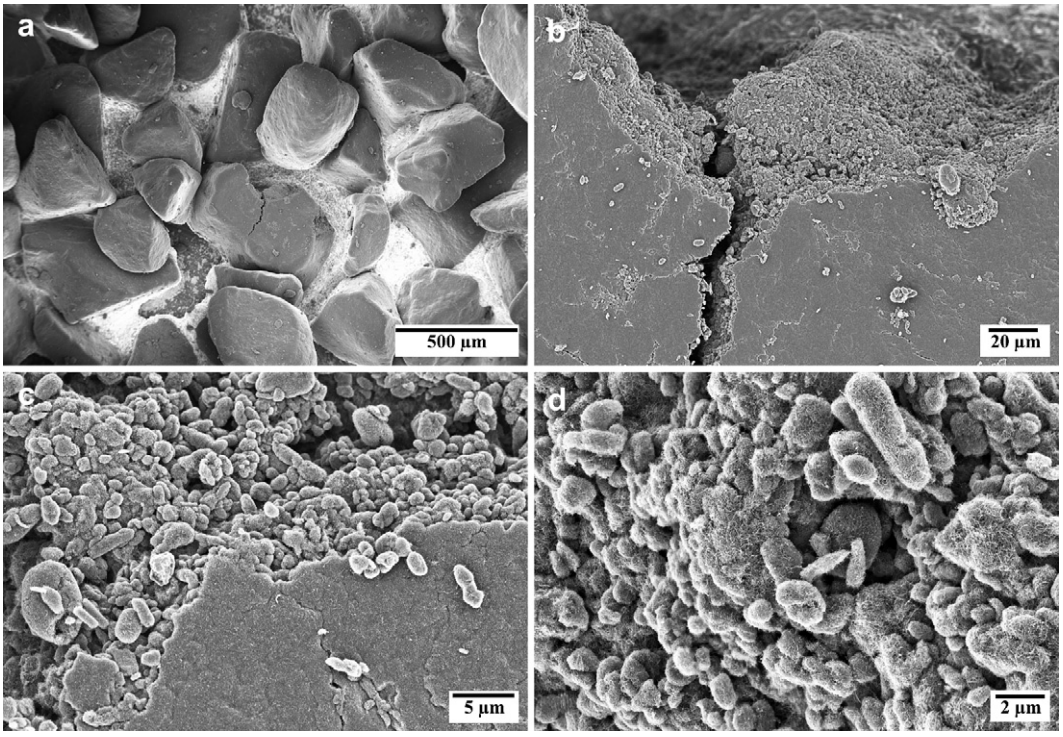

Fig. 2. SEM images of Baytubes C150HP (a) as delivered agglomerates; (b, c, and d) higher magnifications of a fractured agglomerate.

agglomerates in the smallest diameter class (1–10 μm), irrespective of mixing time. A difference of at least one order of magnitude in the number of agglomerates of diameter class (1–10 μm) with other diameter classes is observed. Nevertheless, the number of agglomerates from the smallest diameter class (1–10 μm) also decreases with increasing mixing time, and is relatively lower at higher mixing speeds. It should be noted that the size distribution of "as incorporated" agglomerates (Fig. 1) was much broader as compared to what was observed in the melt mixed composites.

To summarise the observations mentioned above, in Figs. 5a and b the area ratio A and number of agglomerates (per mm^2) are plotted versus mixing time.

In Fig. 5a, a distinct difference in the area ratio A of composites produced at different mixing speeds can be seen. With increasing the mixing speed from 50 rpm to 300 rpm, a drastic reduction in un-dispersed agglomerate area occurs at any corresponding mixing time. Secondly, the area of un-dispersed agglomerate also reduces with increasing mixing time; this is more prominent at lower mixing speeds than at high speed (300 rpm). For all mixing speeds above certain mixing time, dispersion gets slower. The number of un-dispersed agglomerates (per mm^2) decreases with increasing mixing time as shown in Fig. 5b. This decrease slows down as the mixing time increases irrespective of mixing speed and seems to approach a plateau value. At high mixing speed this plateau is reached much faster as compared to low mixing speeds. As most of the agglomerates are from the smallest diameter class (1–10 μm) (ref. Fig. 4), perhaps these agglomerates are hardest to disperse. Interestingly, in all cases even after 40 min of mixing, un-dispersed agglomerates are present.

It is obvious from Fig. 5a that the initial state of evolved morphology (after 30 s) and its further development with time depends on the mixing speed. To analyse the extent of morphology development from initial mixing time at all speeds, the relative change in the area ratio ($(1 - A(t)/A_0)$, i.e. the decrease in area $A(t)$ of un-dispersed agglomerates at any time t, with reference to the area (A_0) at 30 s of mixing) is plotted versus mixing time in Fig. 6. Furthermore, certain mixing energy was incorporated to realise agglomerate dispersion. This applied specific mixing energy during the mixing process is plotted versus mixing time in Fig. 7.

It can be seen from Fig. 6 that there is a fast improvement in the dispersion at 300 rpm with 80% of change realised in 7 min and further change in the area ratio is quite slow. At lower mixing speeds of 100 rpm and 50 rpm, the relative change in the area ratio is 80% and 60% respectively, after 40 min of mixing time. This indicates that at lower mixing speeds the rate of dispersion is slower. Obviously, at 300 rpm, the applied specific mixing energy is much higher than at other mixing speeds as shown in Fig. 7. Further, the difference in the mixing energy at 50 and 100 rpm is relatively smaller.

In Fig. 8, the relative change in area ratio is plotted versus the specific mixing energy. It is obvious that the relative change in area ratio increases with increasing specific mixing energy; but it should be noticed that 80% of the change can be achieved with relatively low input of energy. On the other hand, it seems to be very difficult to reduce the remaining 20% of the original area ratio. At a given value of specific mixing energy, the relative change in area ratio is slightly higher at low mixing speed (50 rpm and 100 rpm) than at high mixing speed. However, in general the values resulting from different mixing speeds can be approximated by a common curve.

The different shear stresses impacting the composite material inside the compounder are dependent on mixing speeds. These shear stresses are transferred over the matrix polymer melt onto the agglomerates, resulting in their dispersion. In case of dispersion of CB in simple shear flow as mentioned earlier, Rwei et al. [16–18] state that at low values of shear stress, CB disperses by erosion mechanism which needs a long time, whereas at high shear stress, CB disperses by rupture mechanism which needs comparatively less time. Therefore, it can be speculated that at high mixing speed resulting in high shear stresses, the MWNT agglomerates undergo dispersion mainly by rupture mechanism; and at low speed corresponding to low shear stresses MWNT agglomerates mainly experience dispersion by erosion mechanism.

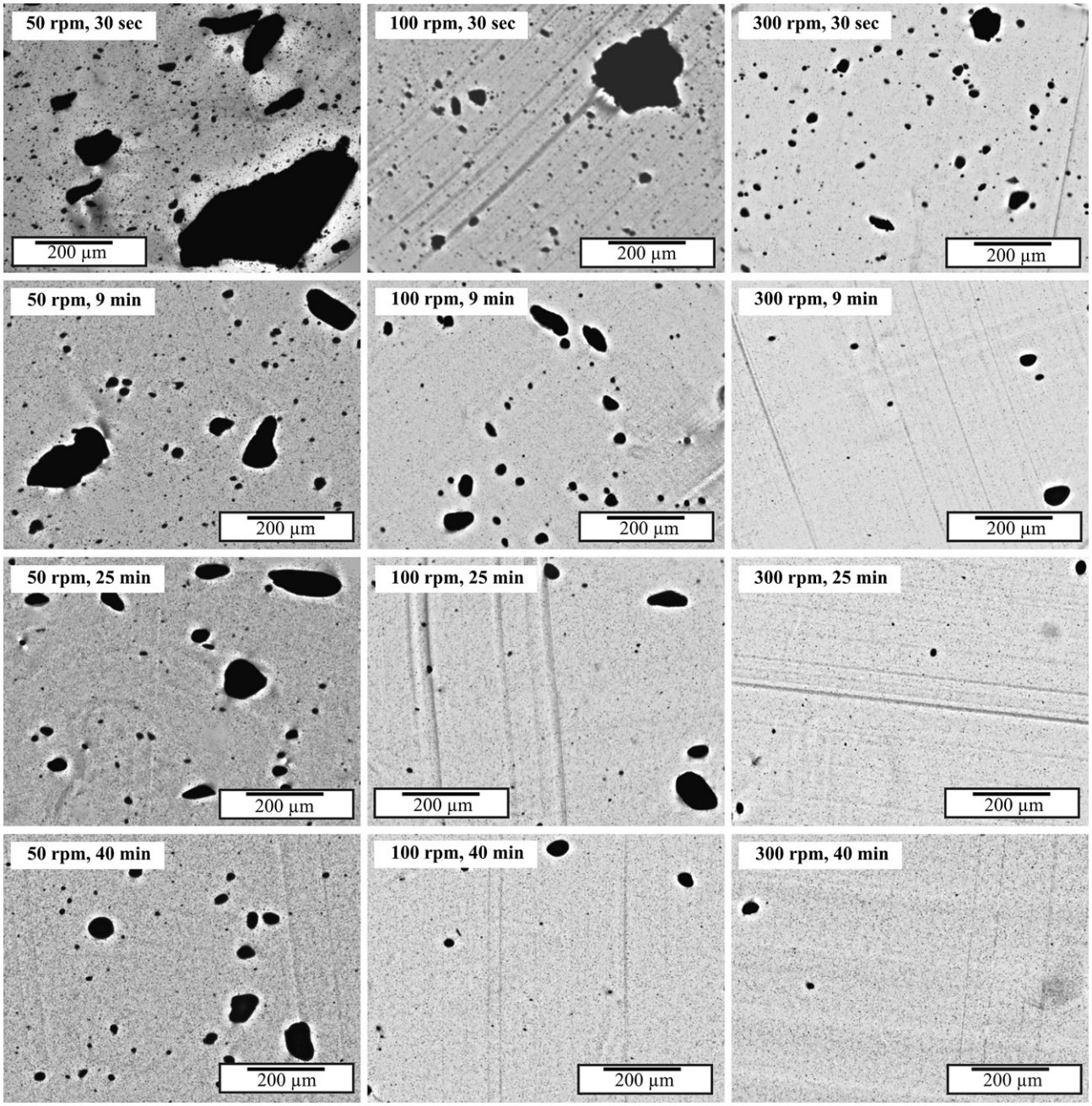

Fig. 3. Optical micrographs illustrating the state of MWNT agglomerate dispersion at different mixing speeds and times.

It is reasonable to expect that both mechanisms of dispersion should exist during any melt mixing operation as the one discussed in this work and all agglomerates are subjected to simultaneous dispersion by erosion and rupture mechanisms. Nevertheless, depending on compounding conditions, one mechanism could dominate the other.

TEM images illustrating typical features of the agglomerate dispersion mechanisms are shown in Fig. 9a and b. During rupture mechanism, cracks propagating through the agglomerate as shown in Fig. 9a, will lead to smaller agglomerates of different sizes. During dispersion by erosion mechanism (see Fig. 9b), free tubes as well as small fragments and agglomerates are eroded from the surface of bigger agglomerates. This mechanism can prevail irrespective of the size of the parent agglomerates.

In Fig. 10, a schematic model is presented to describe the dispersion process of MWNT agglomerates by rupture and erosion dominant mechanisms. In rupture dominant mechanisms, the bigger agglomerates are broken down quite fast into smaller ones, which can be reduced further in size. However, the cohesive strength of agglomerates itself could be a limiting factor. In erosion dominant mechanism, the size of agglomerates is reduced in comparatively longer time and dispersion is driven mainly by melt infiltration. Nevertheless, to avoid floating of agglomerates without dispersion, certain critical screw speeds are always desired for having some flow field acting on agglomerates and also to distribute the tubes and fragments separated from the agglomerates.

Each dispersion mechanism has certain advantages and disadvantages. Rupture mechanism is fast but causes breakage of the dry

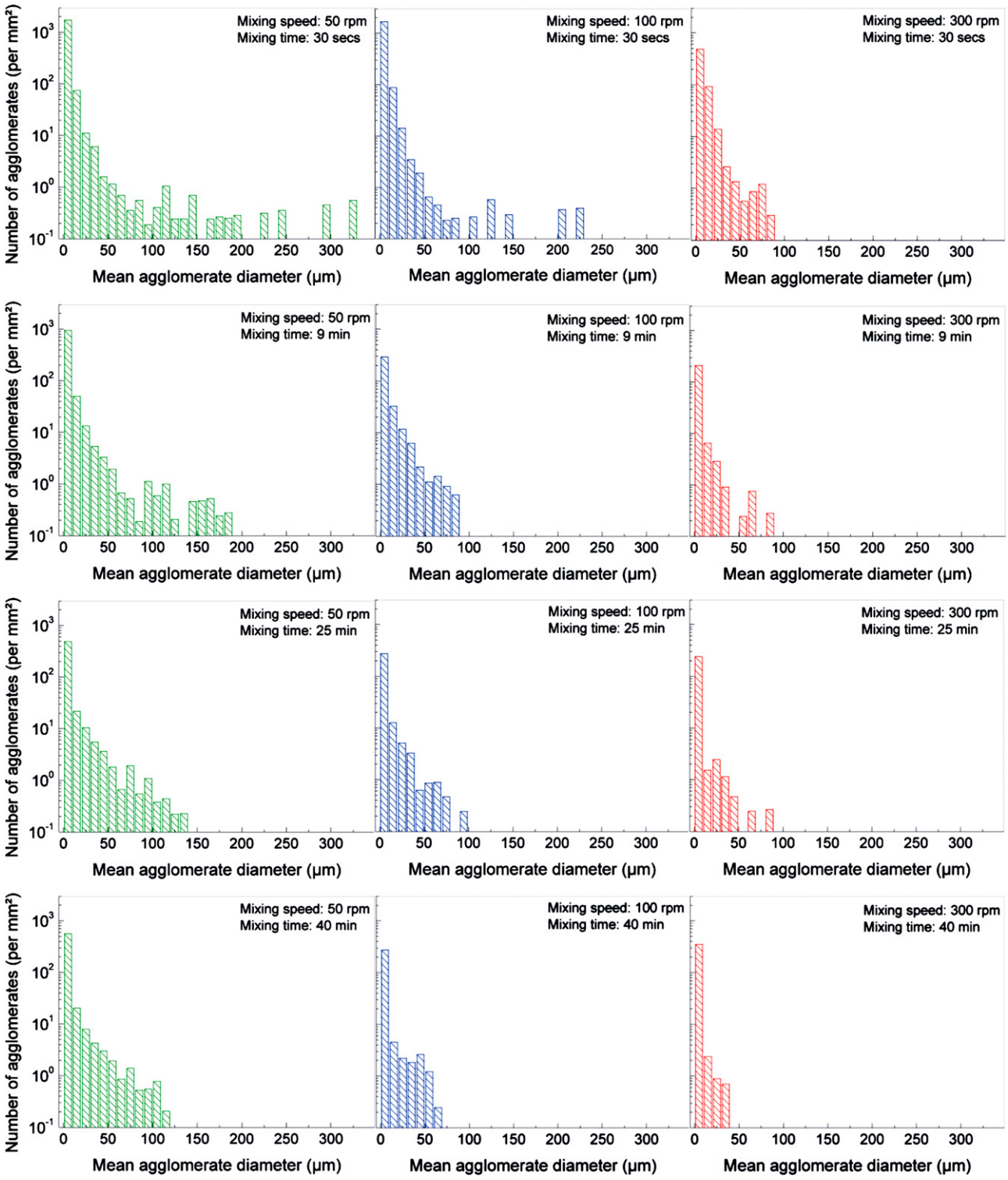

Fig. 4. Size distribution of un-dispersed agglomerates observed in polycarbonate with 1 wt% MWNT composites prepared at different mixing speeds and times.

agglomerates core and hence the undesired breakage of tubes (mainly on defect locations) reducing their aspect ratio. The erosion mechanism is slow but leads to well infiltrated agglomerates and is not expected to cause damage to the tubes.

A complete agglomerate free composite with separated, well dispersed tubes shown as the last step by erosion or rupture dominant mechanism in Fig. 10 could not be achieved in the presented work. Huang et al. [31] reported a mixing time of 100 min for achieving a stable and complete dispersion of 1 wt% MWNT in PDMS, by applying a mixing speed of 1000 rpm in their container mixer having a blade stirrer.

As mentioned in the introduction, Hansen et al. [25] and Ottino et al. [26] stated a criteria for rupture and erosion based on the fragmentation number. As per the criteria, if the applied hydrodynamic stress is smaller than the cohesive strength, particles undergo dispersion by erosion mechanism; and if hydrodynamic

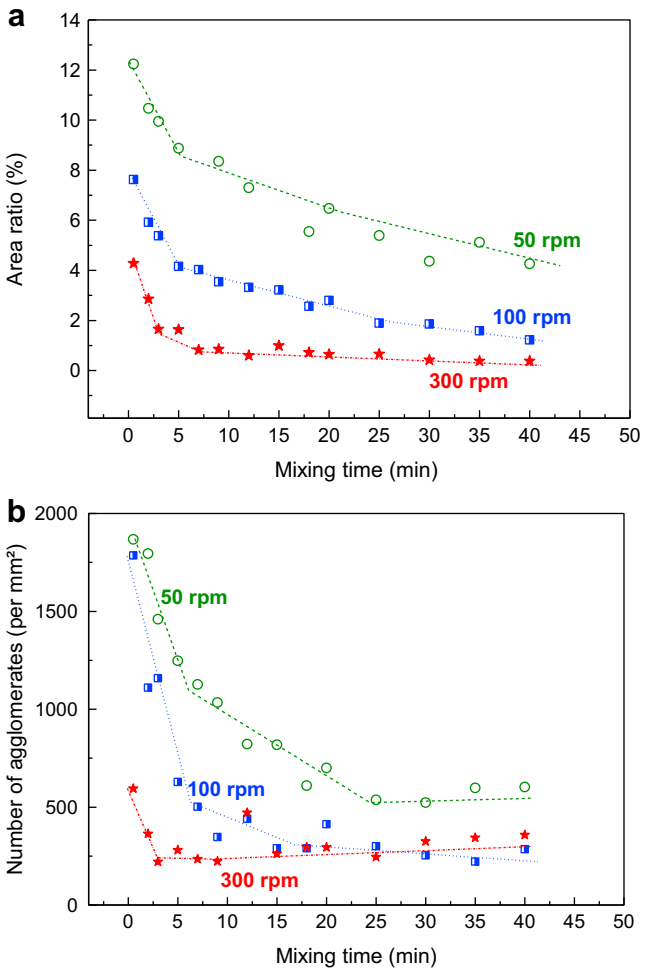

Fig. 5. (a) Area ratio *A* vs. mixing time at different mixing speeds (lines are drawn to guide eyes). (b) Number of agglomerates (per mm^2) vs. mixing time at different mixing speeds (lines are drawn to guide eyes).

stresses are higher, particles undergo dispersion by rupture mechanism. The estimation of the cohesive strength of MWNT agglomerates is not discussed so far in literature as per our knowledge. In our approach [32], these MWNT agglomerates were dispersed in a polycarbonate melt, and were subjected to different

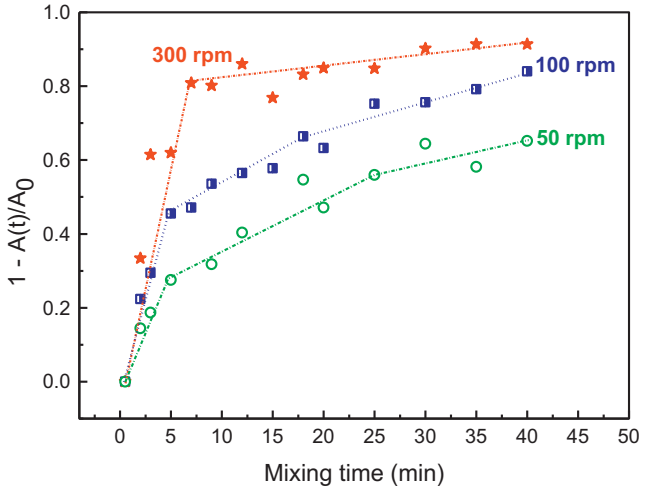

Fig. 6. Relative change in the area ratio vs. mixing time at different mixing speeds (lines are drawn to guide eyes).

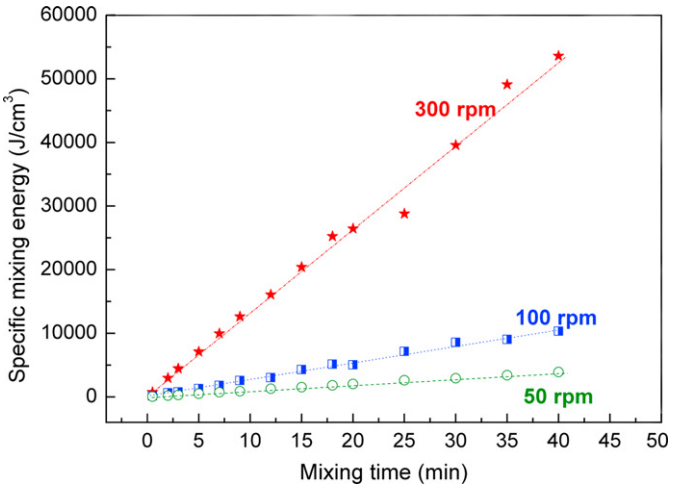

Fig. 7. Specific mixing energy vs. mixing time incorporated at different mixing speeds (lines are drawn to guide eyes).

shear stresses. The average cohesive strength or agglomerate strength was determined from the evolution of un-dispersed agglomerate area change versus shear stress and was found to be approximately 0.3 MPa. Moreover, there is a shear stress distribution inside the compounder, with maximum hydrodynamic stress prevailing in between the screws and the barrel of the compounder. These maximum hydrodynamic stresses at 50, 100, and 300 rpm were calculated to be approximately 0.14 MPa, 0.28 MPa, and 0.67 MPa, respectively. As the MWNT material has very broad initial particle size distribution, which undergoes big change during mixing, it is difficult to state that at 50 rpm there are purely erosion conditions and at 300 rpm there are purely rupture conditions. In addition, in such a compounder, MWNT agglomerates are expected to disperse by both mechanisms. From the concept of fragmentation number, it is not possible to estimate the parts of dispersion by rupture and erosion mechanism. Thus, a new model is proposed to address the issue of quantification of dispersion mechanisms.

3.2.2. *Quantification of the dispersion mechanisms*

In the following section, a model is proposed to evaluate the shares of dispersion by rupture and erosion mechanism during melt mixing under different conditions. This knowledge might be helpful in finding suitable compounding condition to produce

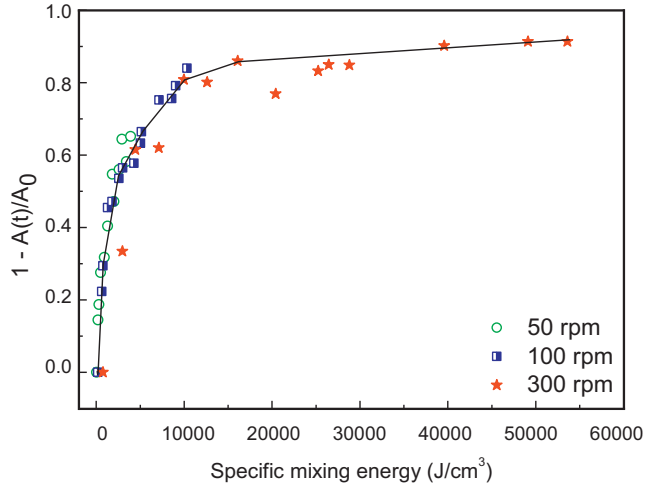

Fig. 8. Relative change in the area ratio vs. specific mixing energy at different mixing speeds (line is drawn to guide eyes).

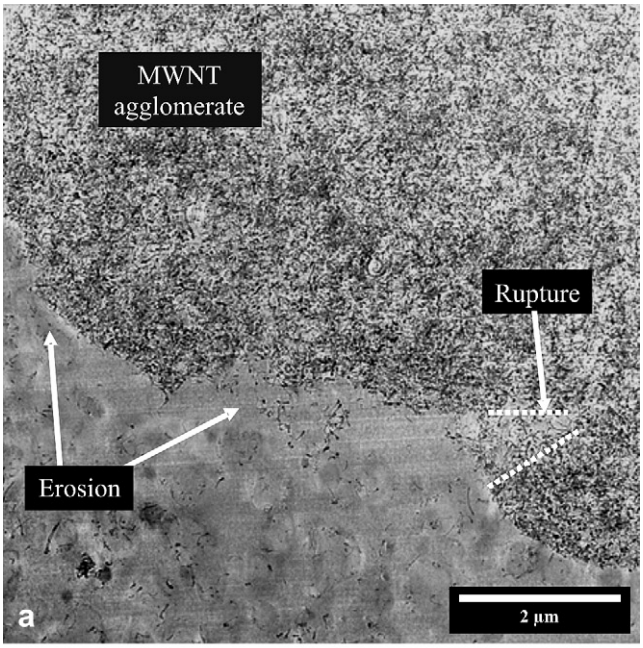

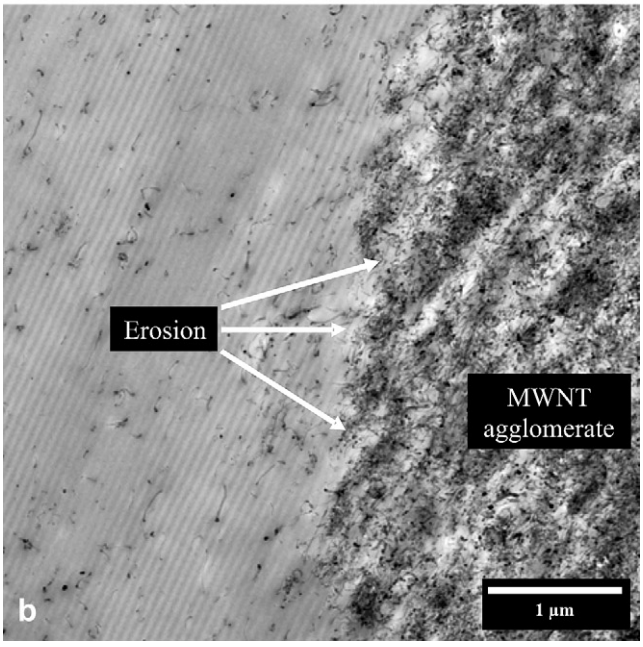

Fig. 9. Illustration of a) rupture and erosion and b) erosion of agglomerates (dotted lines in Fig. 9a indicates region of crack propagation).

composites free of primary agglomerates as it is desired especially for enhancement of mechanical properties of the nanocomposites. As mentioned in the introduction, several models concerning filler dispersion are discussed in literature for rupture and erosion mechanisms; however, those models assume either erosion or rupture. Potente et al. [27] and Lozano et al. [28] considered both mechanisms, however, no direct quantification of the extent of dispersion mechanisms was done. So far, by our knowledge, in literature no method or model is developed which addresses the extent of both mechanisms participating in a real mixing process.

In order to quantify the dispersion mechanisms, we consider the morphology evolved at the lowest mixing time (30 s) applied in the mixing study as the initial state of MWNT agglomerate dispersion and agglomerate diameter distribution. Thus, A_0 represents the area ratio A, at 30 s; and A_t the area ratio A, at time t.

In Fig. 11, a scheme illustrates the reduction in the (un-dispersed) agglomerate area ratio from A_0 to A_t under the action of the applied shear stress ($\tau_{applied}$) with mixing time t. In the model proposed here, it is assumed that irrespective of the dispersion mechanism, the time dependent decrease in the un-dispersed MWNT agglomerate area (area ratio) is directly proportional to the un-dispersed agglomerate area (area ratio) and the applied shear stress:

$$-\frac{dA}{dt} \propto A\cdot\tau_{applied} \quad \left(\tau_{applied} = K'\cdot\eta\cdot\dot{\gamma}\right) \tag{1}$$

$$-\frac{dA}{dt} = k\cdot A\cdot\tau_{applied} \tag{2}$$

where, k is a constant of proportionality, called as "constant of dispersion kinetics". The calculation of the applied shear stress ($\tau_{applied}$) is given in the Appendix. Solving the ordinary differential equation (2) with the boundary condition of an initial area ratio A_0 at time $t = 30$ s leads to the area A_t at time t:

$$A_t = A_0\cdot\exp\left(-k\cdot\tau_{applied}\cdot t\right) \tag{3}$$

The agglomerates are subjected to dispersion by both rupture and erosion mechanism, thereby reducing the initial area ratio A_0 to a final area A_t after mixing time t. In the following, we assume that the initial part of the area A_0 can be divided into two parts; part "a" that undergoes dispersion by erosion and a part "b" that undergoes dispersion by rupture mechanism (with a termed as the coefficient of erosion and b termed as the coefficient of rupture (equation (4))). These two fractions of initial area ratio are the base for the evolution of the area ratio A_t^E and A_t^R formed by rupture and erosion mechanism after time t (equation (5)).

$$A_0 = a\cdot A_0 + b\cdot A_0 \tag{4}$$

and

$$A_t = A_t^E + A_t^R \tag{5}$$

Thus, equation (3) can be re-written for A_t^E and A_t^R as:

$$A_t^E = a\cdot A_0\cdot\exp\left(-k^E\cdot\tau_{applied}\cdot t\right) \tag{6}$$

similarly,

$$A_t^R = b\cdot A_0\cdot\exp\left(-k^R\cdot\tau_{applied}\cdot t\right) \tag{7}$$

Here, k^E and k^R are the constants of erosion and rupture kinetics, respectively. Substituting equations (6) and (7) in equation (5) leads to:

$$A_t = a\cdot A_0\cdot\exp\left(-k^E\cdot\tau_{applied}\cdot t\right) + b\cdot A_0\cdot\exp\left(-k^R\cdot\tau_{applied}\cdot t\right) \tag{8}$$

In further evaluation, the used value of $\tau_{applied}$ is assumed as the maximum shear stress prevailing between the screws and the barrel of the compounder. Additionally, we assume that this maximum shear stress is constant during the mixing process. Hence equation (8) contains four unknown parameters a, b, k^E, and k^R. Considering the complexity of the subject, certain additional assumptions are necessary to estimate the values of these unknown quantities.

3.2.2.1. Evaluation of k^E and k^R. In Section 3.2.1, it is discussed that a broad un-dispersed agglomerate diameter distribution is present

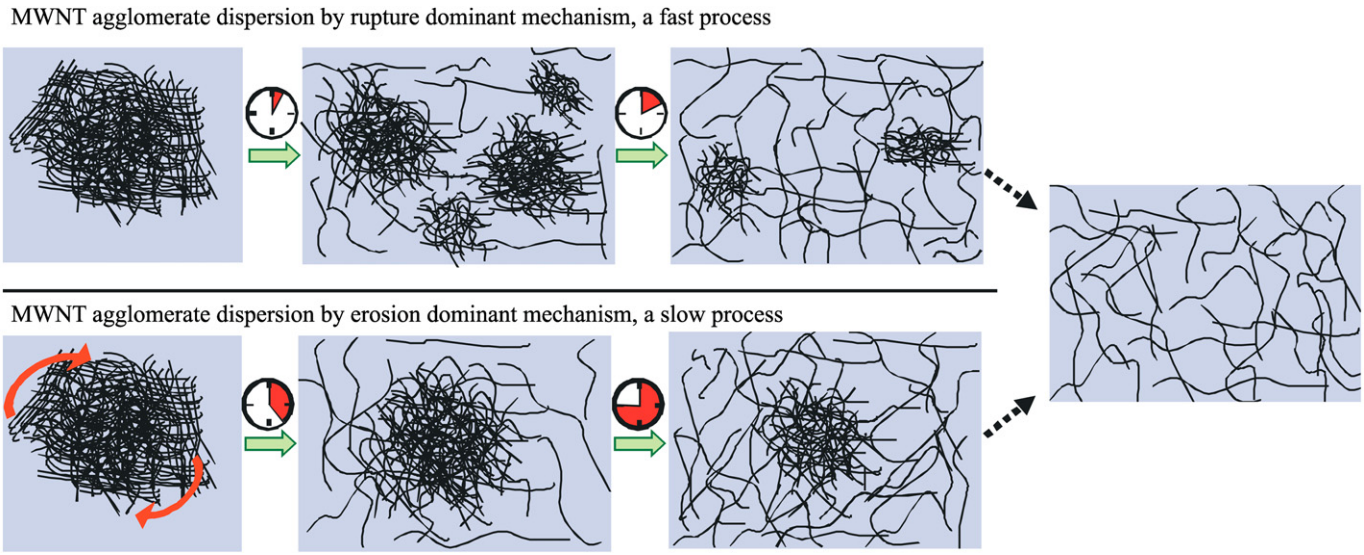

Fig. 10. Schematic descriptions of MWNT agglomerate dispersion mechanisms.

in the composites at initial mixing time, which undergoes continuous change. The bigger agglomerates are found to be dispersing faster than the smaller ones and the smaller ones are found to be very hard to disperse even at high input of energy (ref. Figs. 4, 5b and 8).

Based on those findings, for the evaluation of k^E and k^R we will therefore consider the changes in the area of agglomerates from certain diameter classes.

Assumptions:

1. The agglomerates in the particle diameter class ~1–10 μm (corresponding to the length of MWNT) are the smallest possible objects to be measured in light microscopy. Since these small agglomerates are assumed to consist of highly packed structures with entangled MWNT (see Fig. 2) they have a very high strength (estimated to be 33.4 MPa, see Appendix). As this magnitude of shear stress is not realised in the compounder during the experiments it may be assumed that agglomerate in that diameter class do not undergo rupture. Since their area ratio is decreasing with mixing time there is a high probability that they undergo dispersion by erosion mechanism only. The decrease in the area ratio of these small agglomerates, A_0^{Small} along the mixing time to A_t^{Small} can be written as equation (6):

$$A_t^{\text{Small}} = A_0^{\text{Small}} \cdot \exp\left(-k^E \cdot \tau_{\text{applied}} \cdot t\right) \tag{9}$$

2. All other agglomerates (above 1–10 μm class) are assumed to be formed by the small agglomerates from 1 to 10 μm class (as it was indicated by Fig. 2) and thus have a relatively weaker agglomerate strength (see Appendix). Under the applied mixing condition, sufficient shear stresses are present for rupture of these agglomerates into smaller ones. The decrease in the area ratio of these big agglomerates, A_0^{Big} with mixing time to A_t^{Big} can be written as equation (7):

$$A_t^{\text{Big}} = A_0^{\text{Big}} \cdot \exp\left(-k^R \cdot \tau_{\text{applied}} \cdot t\right) \tag{10}$$

It is mentioned earlier that all particles are subjected to dispersion by erosion and rupture mechanism simultaneously. Although the constants of erosion and rupture kinetics, i.e. k^E and k^R evaluated from equations (9) and (10), are calculated using the agglomerate area from specific diameter classes, they are assumed to be applicable for all agglomerates.

Since it is assumed that the constants of erosion and rupture kinetics are valid for all three mixing speeds, in Figs. 12 and 13 the area ratio of small (1–10 μm) and big (above 10 μm) agglomerates for all mixing speeds and times is plotted versus $\tau_{\text{applied}} \cdot t$. To evaluate k^E and k^R as constants of erosion and rupture kinetics, curve fitting is carried out using Origin 8.0 and by applying the method of the lowest value of the root mean square error, following equation (11):

$$y = B' \cdot \exp\left(-\frac{x}{\alpha}\right) + y_0 \tag{11}$$

From equations (9) and (10), $1/\alpha$ corresponds to k^E or k^R.

The values of k^E and k^R are evaluated to be 1.5 E − 8 $(\text{Pa s})^{-1}$ and 3.6 E − 9 $(\text{Pa s})^{-1}$. The value of k^R is smaller by one order of magnitude than k^E supporting the fact that larger agglomerates disperse faster than smaller ones.

3.2.2.2. Evaluation of a and b. Following equation (8) and by using the values of k^E and k^R, the coefficients of erosion (a) and rupture (b)

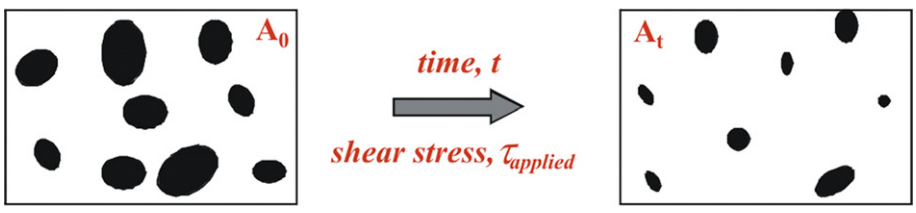

Fig. 11. Scheme showing reduction in agglomerate area ratio from A_0 to A_t.

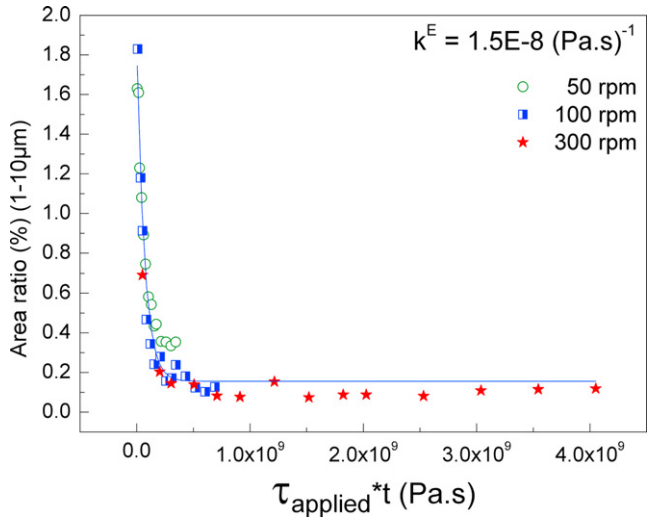

Fig. 12. Area ratio of small agglomerates (1–10 μm) vs. $\tau_{applied}\cdot$time (line represents a fit of equation (11)).

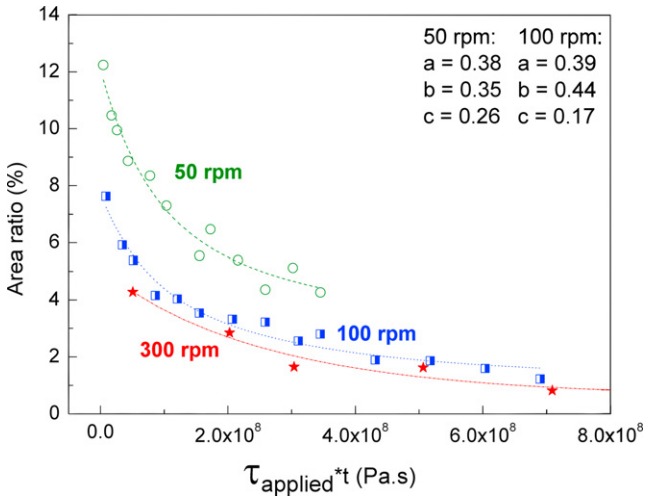

Fig. 14. Area ratio vs. $\tau_{applied}\cdot$time (lines represent fits of equation (12)).

can be evaluated. The un-dispersed agglomerate area ratio is plotted versus $\tau_{applied}\cdot t$ (up to 7×10^8 Pa s) in Fig. 14, and for 300 rpm Fig. 15 shows the range of $\tau_{applied}\cdot t$ up to 4×10^9 Pa s.

Curve fitting is carried out using Origin 8.0 and applying the method of the lowest value of the root mean square error, following the equation (12):

$$y = B'\cdot\exp\left(-\frac{x}{\alpha_1}\right) + B''\cdot\exp\left(-\frac{x}{\alpha_2}\right) + y_0 \qquad (12)$$

Comparing with equation (8), B' corresponds to $a\cdot A_0$, B'' corresponds to $b\cdot A_0$, $1/\alpha_1$ and $1/\alpha_2$ corresponds to k^E and k^R respectively and y_0 is an offset parameter. Apart from the area that undergoes dispersion by rupture and erosion, some agglomerate area remains unaffected or not dispersed at all. This part of area corresponds to y_0 (labelled as c).

From the curve fitting for all mixing speeds, the amount of initial area that undergoes dispersion by erosion (a), rupture (b) and the part that remains un-dispersed (c) are evaluated. At 50 rpm, the dispersion by erosion mechanism is 38%, and as the mixing speed is increased to 100 rpm this value remains stable. However, as mixing speed is increased up to 300 rpm the fraction of dispersion by erosion drops to 5%. Conversely, dispersion by rupture mechanism increases from 35% at 50 rpm to 44% at 100 rpm and to 83% at 300 rpm. The un-dispersed part decreases from 27% at 50 rpm to 12% at 300 rpm.

The different fractions of erosion and rupture in the dispersed part are plotted versus. mixing speed in Fig. 16. The dispersion by erosion mechanism at 50 rpm is 52%, which is reduced to 6% at 300 rpm. Conversely, dispersion by rupture mechanism increases from 48% at 50 rpm to 94% at 300 rpm.

At low mixing speeds of 50 rpm and 100 rpm both mechanisms govern MWNT agglomerate dispersion as the shares of both dispersion mechanisms are nearly the same. At 300 rpm, the rupture mechanism is dominant. Using the selected PC and MWNT it seems that dispersion by purely erosion mechanism is not possible when performing melt mixing in the microcompounder at 280 °C.

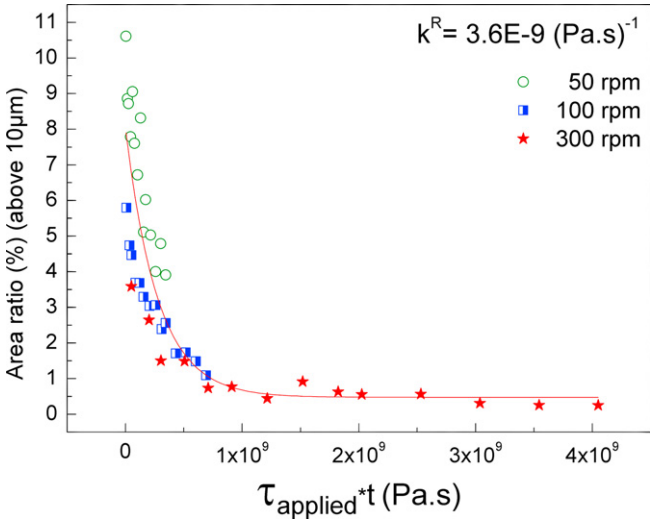

Fig. 13. Area ratio of big agglomerates (above 10 μm) vs. $\tau_{applied}\cdot$time (line represents a fit of equation (11)).

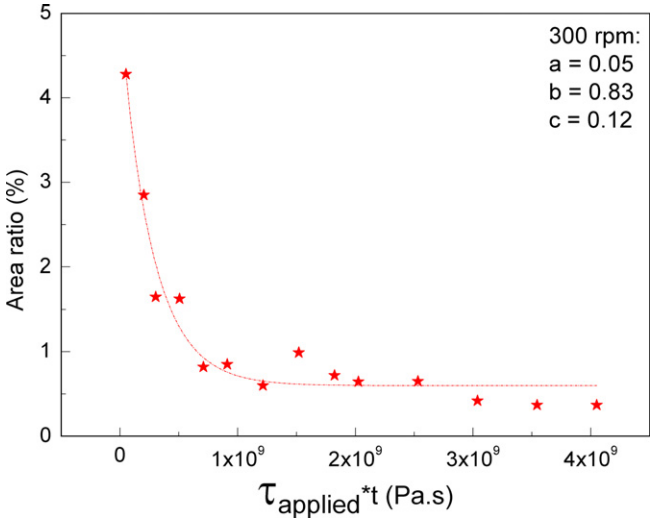

Fig. 15. Area ratio vs. $\tau_{applied}\cdot$time (for 300 rpm) (line represents a fit of equation (12)).

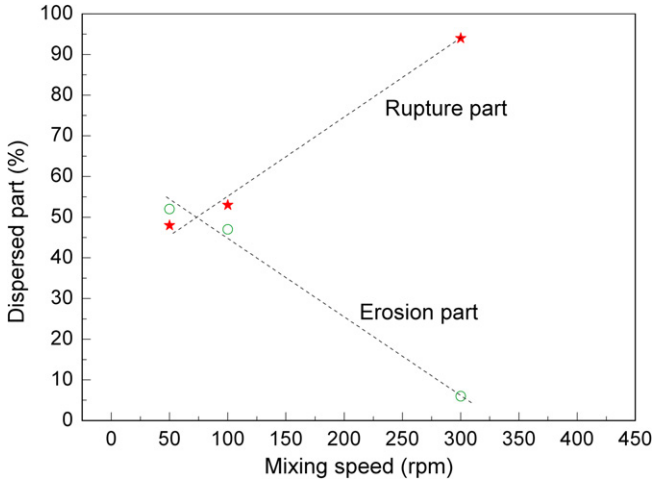

Fig. 16. Share of erosion and rupture in the dispersed part of agglomerate vs. mixing speed (lines are drawn to guide eyes).

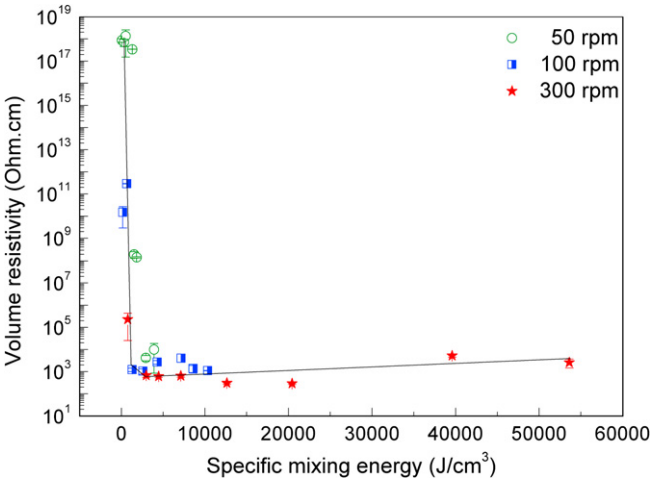

Fig. 18. Volume resistivity vs. specific mixing energy (line is drawn to guide eyes).

3.3. Electrical volume resistivity

Resistivity measurements were carried out to get information about the state of electrical network formation. The volume resistivity of the composites is plotted versus mixing time in Fig. 17, versus specific mixing energy in Fig. 18, and versus area ratio in Fig. 19. As shown in Fig. 17, depending on the employed mixing speeds, the electrical volume resistivity values decreases with increasing mixing time until a plateau is reached. At higher mixing speed, this plateau is reached faster as compared to lower mixing speeds.

Plotting resistivity versus specific mixing energy and area ratio (Figs. 18 and 19) indicates common curves for all mixing speeds. The volume resistivity versus mixing energy decreases drastically till a certain resistivity plateau is reached at about 1400 J/cm^3 and there is no further decrease with increasing specific mixing energy. Interestingly, this result is in agreement with earlier reported works [8,33].

Concerning the dependency of resistivity on area ratio two plateaus can be observed. At agglomerate area ratios above 7%, corresponding to low mixing energies, the electrical resistivity of the composites is altogether dominated by the matrix system. Below approximately 4% the electrical resistivity is dominated by the filler. These data points can be assigned to high mixing energies. Both plateaus are separated by a transition region where the electrical resistivity changes over approximately 14 orders of magnitude. This is a very interesting observation since it is commonly assumed that the electrical resistivity decreases with increasing filler dispersion. However, our results clearly indicate, that this assumption holds only in a limited transition range. In the selected system of 1 wt% Baytubes C 150HP in Makrolon 2205 and with an used section thickness of 20 microns for transmission light microscopy this range was found to be between 4% and 7% agglomerate area ratio, corresponding to mixing energies 1400 J/cm^3 and 500 J/cm^3, respectively.

This critical phenomenon can be explained as following: With decreasing area ratio the amount of dispersed nanotubes increases. At a critical amount of dispersed nanotubes the percolation concentration is reached and the electrical resistivity decreases substantially. Above the percolation concentration i.e. with further nanotube dispersion the changes in resistivity become less dependent on the state of dispersion since the electrical network is already well established. The contribution of the remaining agglomerates to the overall composite conductivity seems to be negligible as their occupied volume is comparatively small. The distance between remaining agglomerates is much larger then the

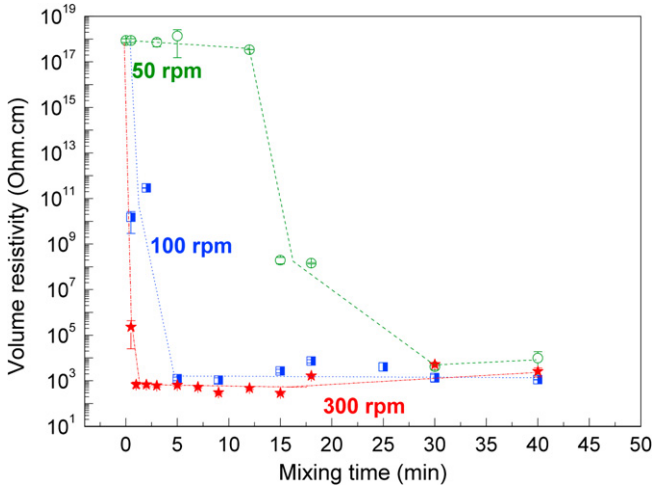

Fig. 17. Volume resistivity vs. mixing time at different mixing speed (lines are drawn to guide eyes).

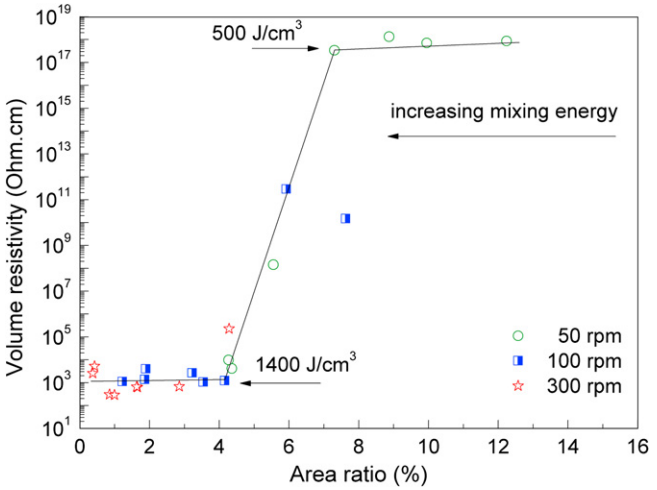

Fig. 19. Volume resistivity vs. agglomerate area ratio (line is drawn to guide eyes).

nanotube length and the percolation structure is clearly determined by the dispersed tubes between the agglomerates.

Since under all mixing conditions used remaining agglomerates are existent, but below 4% area ratio conductivity is reached and one can conclude that the 1 wt% loading used is above the percolation threshold. With proper dispersion percolation below 1 wt% can be reached. Furthermore, it can be assumed that the location of the transition range (as seen in Fig. 19) depends on the amount of filler since the fraction of nanotubes that has to be dispersed in order to reach percolation increases with decreasing total filler content. Thus, a shift towards lower area ratio can be expected when lowering the nanotube content.

4. Summary and conclusions

The kinetics of MWNT agglomerate dispersion was investigated during melt compounding in a small scale mixer with PC and 1 wt% MWNT at three different mixing speeds (50, 100, and 300 rpm) and with increasing mixing time (up to 40 min). The states of evolved MWNT agglomerate dispersion as assessed by image analysis of optical transmission micrographs strongly depend on the mixing speed. MWNT agglomerate dispersion is faster and better in composites prepared at higher mixing speeds than those prepared at low mixing speeds. It was also found that bigger agglomerates disperse faster than smaller ones. In a melt compounder agglomerates are subjected to dispersion by both erosion and rupture mechanisms and the share of each mechanism is estimated using a new model based on first order kinetics. The model considers the agglomerate area ratio in dependence on the product of applied shear stress and time. It was found that the share of dispersion by erosion mechanism decreases and the share of dispersion by rupture mechanism increases with increasing mixing speed. However, already at the lowest mixing speed applied in the investigations rupture and erosion have about the same extent, indicating that in most melt extrusion processes rupture mechanism can be assumed to be dominant at higher mixing speeds.

Interestingly, for all mixing conditions selected no complete dispersion of the nanotube material used could be achieved. This may be related to the very high agglomerate strength based on the comparatively low porosity of this type of nanotube agglomerates (see measurement in the Appendix). For other nanotube materials having higher porosity values the agglomerate strength may be lower leading to lower un-dispersed parts and faster dispersion kinetics. In addition, also the nanotube length of the starting nanotube material may influence the kinetic and the share of rupture and erosion during dispersion.

Further, electrical resistivity of composites was found to decrease with mixing energies up to about 1,400 J/cm^3. At higher mixing energies (up to about 55,000 J/cm^3) reached by either enhancing mixing speed or mixing time a plateau with low resistivities is established. Considering the relationship between dispersion and electrical resistivity a critical behaviour was observed since the percolation is dominated by the fraction of dispersed nanotubes. Below and above this percolation range the influence of the state of nanotube dispersion, as expressed by the agglomerate area ratio, was found to be only marginal. To derive a model of more generality than in the presented investigations the amount of dispersed nanotubes and thus the real percolation concentration has to be determined more precisely, e.g. using methods as presented in [34].

Acknowledgement

We would like to thank Bayer MaterialScience AG, Leverkusen (Germany) for supplying polycarbonate and Baytubes® C150HP. We would like to thank Dr. Beate Krause and Mr. Uwe Geißler for carrying out MWNT particle size analysis, Miss Manuela Heber and Miss Uta Reuter for helping with TEM investigation, and Miss Monika Henze and Mr. Helfried Kunath for general assistances. The research and development project is funded by the German Federal Ministry of Education and Research (BMBF) within the Framework Concept "Research for Tomorrow's Production" (funding number 02PU2392) and managed by the Project Management Agency Karlsruhe (PTKA).

Appendix

- Calculation of hydrodynamic stress $\tau_{applied}$ (Section 3.2.2.1, equation (1)):

$$\tau_{applied} = K' \cdot \eta \cdot \dot{\gamma} \tag{a1}$$

- K' (for spherical particles) = 2.5 [35]
- Evaluation of shear rate $\dot{\gamma}$ using ref [36]:

$$\dot{\gamma} = \frac{\pi \cdot (D - 2\delta) \cdot N}{\delta} \tag{a2}$$

Here, D is screw diameter (9.725 mm) and δ is screw clearance with barrel (100 μm), N is mixing speed in rps; viscosity η values at applied shear rates $\dot{\gamma}$ are from [37].

- Agglomerate strength (σ) calculation (Section 3.2.2.1, assumptions 1 and 2):

Agglomerate strength, σ or cohesive strength of agglomerates are calculated using Rumpf equation (equation (a3)) [38]. This equation states that the cohesive strength of the agglomerates depends on the size of the particles forming the agglomerates.

a) Rumpf equation for spherical particles:

$$\sigma = \frac{(1 - \varepsilon)}{\varepsilon} \frac{F}{a^2} \tag{a3}$$

For all convex shaped particles, equation (a3) is written as equation (a4) [38].

$$\sigma = (1 - \varepsilon) k \frac{F}{A} \tag{a4}$$

Here, σ is agglomerate strength, ϵ is porosity, F represents adhesive forces which in case of dry agglomerates are predominantly Van der Waals force between particles, a is the diameter of particles forming the agglomerates, k is the coordination number of particles forming agglomerate, and A is the surface area (of particles forming agglomerates) is $2\pi R^* L$ (for rods).

b) Van der Waals forces between two spheres (equation (a5)) and rods/cylinders (equation (a6)) near to touching from Ref. [39]:

$$F_{Sphere} = \frac{-H}{6D^2} \left(\frac{R_1 R_2}{R_1 + R_2} \right) \tag{a5}$$

$$F_{Cylinder} = \frac{-H}{8\sqrt{2}} \frac{L}{D^{5/2}} \left(\frac{R_1 R_2}{R_1 + R_2} \right)^{1/2} \tag{a6}$$

Here, H is Hamaker's constant of MWNT (60 E − 20 J, [40]), D is inter particle distance (assumed 0.4 nm (inter graphite layer separation)), L is length of particle, R is radius of particle (in our calculations, $R_1 = R_2 = R$), ϵ is porosity of MWNT agglomerate (0.85,

measurement and calculation explained below), and k is coordination number (10 for rigid rods with an aspect ratio of 100 and packed with maximum density [41], for flexible fibres/MWNT coordination number values might be much larger).

c) Agglomerate strength (σ) of smaller agglomerates (1–10 μm), made up by individual tubes, is calculated using equations (a4) and (a6). Here, using $R = 7$ nm (radius of nanotube) and $L = 1$–10 μm (length of nanotube) [29] leads to $\sigma = 33.4$ MPa.

Agglomerate strength (σ) of larger agglomerates (above 10 μm), consisting of cylindrical shaped smaller agglomerates; is calculated by applying equations (a4) and (a6). Here, $R = 0.5$–5 μm (radius of smaller agglomerates, assumed) and $L = 1$–10 μm (length of smaller agglomerates, assumed) leads to $\sigma = 1.25$–3.9 MPa.

Agglomerate strength (σ) of larger agglomerates (above 10 μm), consisting of spherical shaped smaller agglomerates; is calculated by applying equations (a3) and (a5). Here, $a = 1$–10 μm (diameter of smaller agglomerates, assumed) and $R = 0.5$–5 μm (radius of smaller agglomerates) leads to $\sigma = 2.75$–27.5 kPa.

Depending upon arrangements σ of large agglomerates can vary between 2.75 kPa and 3.9 MPa.

[Remark: All calculated values of MWNT agglomerate strength will be 10 times lower if Hamaker constant of MWNT is taken as 60 E − 21 J [42] (similar to activated carbon [43])].

d) The packing density and thus the porosity of the MWNT agglomerates were determined in the following way: An aluminium cup was filled with the MWNT-powder and vacuum infiltrated with an epoxy resin. After curing the volume fraction of MWNT agglomerates V_A has been estimated by means of thin sections (due to large mean size of the primary agglomerates the area fraction is roughly equal to the volume fraction). With the known masses of epoxy and MWNT as well as the densities, the corresponding MWNT volume fraction of the infiltrated material V_{im} has been calculated. The packing density is given by the ratio of V_{im} and V_A. For Baytubes C150HP, the average agglomerate porosity ϵ is calculated as 0.85. For procedural details see Ref. [42].

References

[1] Takase H. Evaluation and applications of dispersing carbon nanotube in the polymers. In: Hosokawa M, Nogi K, Naito M, Yokoyama T, editors. Nanoparticle technology handbook. Elsevier; 2007. p. 644.
[2] Prashantha K, Soulestin J, Lacrampe MF, Krawczak P, Dupin G, Claes M. Composites Science and Technology 2009;69:1756–63.
[3] Ganss M, Satapathy BK, Thunga M, Weidisch R, Pötschke P, Jehnichen D. Acta Materialia 2008;56(10):2247–61.
[4] Micusik M, Omastova M, Krupa I, Prokes J, Pissis P, Logakis E, et al. Journal of Applied Polymer Science 2009;113(4):2536–51.
[5] Du FM, Scogna RC, Zhou W, Brand S, Fischer JE, Winey KI. Macromolecules 2004;37(24):9048–55.
[6] Masuda J, Torkelson JM. Macromolecules 2008;41(16):5974–7.
[7] Baets J, Godara A, Devaux J, Verpoest I. Composites Part A Applied Science and Manufacturing 2008;39(11):1756–61.
[8] Kasaliwal G, Göldel A, Pötschke P. Journal of Applied Polymer Science 2009;112(6):3494–509.
[9] Manas-Zloczower I. Dispersive mixing of solid additives. In: Tadmor Z, Manas-Zloczower I, editors. Mixing and compounding of polymers: theory and practice. Hanser Publishers; 1994. p. 55–83.
[10] Kao SV, Mason SG. Nature 1975;253(5493):619–21.
[11] Powell RL, Mason SG. Aiche Journal 1982;28(2):286–93.
[12] Shiga S, Furuta M. Rubber Chemistry and Technology 1985;58(1):1–22.
[13] Bolen WR, Colwell RE. Society of Plastics Engineering Journal 1958;14(8):24.
[14] Manas-Zloczower I, Feke DL. International Polymer Processing 1989;4(1):3–8.
[15] Bohin F, Manas-Zloczower I, Feke DL. Chemical Engineering Science 1996;51(23):5193–204.
[16] Rwei SP, Manas-Zloczower I, Feke DL. Polymer Engineering and Science 1990;30(12):701–6.
[17] Rwei SP, Manas-Zloczower I, Feke DL. Polymer Engineering and Science 1991;31(8):558–62.
[18] Rwei SP, Manas-Zloczower I, Feke DL. Polymer Engineering and Science 1992;32(2):130–5.
[19] Boyle J, Manas-Zloczower I, Feke DL. Particle and Particle Systems Characterization 2004;21(3):205–12.
[20] Boyle JF, Manas-Zloczower I, Feke DL. Powder Technology 2005;153(2):127–33.
[21] Pomchaitaward C, Manas-Zloczower I, Feke DL. Chemical Engineering Science 2003;58(9):1859–65.
[22] Scurati A, Feke DL, Manas-Zloczower I. Chemical Engineering Science 2005;60(23):6564–73.
[23] Gopalkrishnan P, Manas-Zloczower I, Feke DL. Powder Technology; 2005:111–9.
[24] Manas-Zloczower I, Nir A, Tadmor Z. Rubber Chemistry and Technology 1982;55(5):1250–85.
[25] Hansen S, Khakhar DV, Ottino JM. Chemical Engineering Science 1998;53(10):1803–17.
[26] Ottino JM, DeRoussel P, Hansen S, Khakhar DV. In: Advances in chemical engineering, vol. 25. Academic Press; 2000. p. 105–204.
[27] Potente H, Kretschmer K, Flecke J. Polymer Engineering and Science 2002;42(1):19–32.
[28] Lozano T, Lafleur PG, Grmela M, Vergnes B. International Polymer Processing 2003;18(1):12–9.
[29] Baytubes C150HP Preliminary datasheet. Bayer MaterialScience AG, Germany; Edition: 2007-05-14.
[30] Stoyan D, Kendall WS, Mecke J. Stochastic geometry and its applications. John Wiley & Sons; 1987.
[31] Huang YY, Ahir SV, Terentjev EM. Physical Review B 2006;73(12):9.
[32] Kasaliwal G, Göldel A, Pegel S, Pötschke P, Heinrich G. Influence of polymer matrix melt viscosity and molecular weight on MWNT agglomerate dispersion. Dresden: Leibniz Institute of Polymer Research Dresden, un published.
[33] Krause B, Pötschke P, Häussler L. Composites Science and Technology 2009;69(10):1505–15.
[34] Pegel S, Pötschke P, Villmow T, Stoyan D, Heinrich G. Polymer 2009;50(9):2123–32.
[35] Elmendorp JJ. Dispersive mixing in liquid systems. In: Rauwendaal C, editor. Mixing in polymer processing. New York: Dekker; 1991.
[36] Rauwendaal C. Important polymer properties. Polymer extrusion. Munich: Hanser Publishers; 1986. p. 181.
[37] Makrolon 2205-viscosity shear rate data. Bayer MaterialScience AG. Global Innovations – Polycarbonates.
[38] Rumpf H. Chemie Ingenieur Technik 1970;42(8):538–40.
[39] Parsegian VA. Van der waals forces, a handbook for biologists, chemists, engineers and physicists. Cambridge University Press; 2006.
[40] Akita S, Nishijima H, Nakayama Y. Journal of Physics D Applied Physics 2000;33(21):2673–7.
[41] Williams SR, Philipse AP. Physical Review E 2003;67(5):9.
[42] Pegel S. Ph.D. thesis. Materials Science Technical University Dresden. Dresden; 2010.
[43] Peukert W, Mehler C, Götzinger M. Applied Surface Science 2002;196(1–4):30–40.